



**HAL**  
open science

## Preliminary results of Pyramide Piston Sensor calibration

Petr Janout, Deborah Malone, Ronald Holzlöhner, Samuel Lévêque, Tomáš Fordey

► **To cite this version:**

Petr Janout, Deborah Malone, Ronald Holzlöhner, Samuel Lévêque, Tomáš Fordey. Preliminary results of Pyramide Piston Sensor calibration. Adaptive Optics for Extremely Large Telescopes 7th Edition, ONERA, Jun 2023, Avignon, France. 10.13009/AO4ELT7-2023-037 . hal-04419889

**HAL Id: hal-04419889**

**<https://hal.science/hal-04419889>**

Submitted on 26 Jan 2024

**HAL** is a multi-disciplinary open access archive for the deposit and dissemination of scientific research documents, whether they are published or not. The documents may come from teaching and research institutions in France or abroad, or from public or private research centers.

L'archive ouverte pluridisciplinaire **HAL**, est destinée au dépôt et à la diffusion de documents scientifiques de niveau recherche, publiés ou non, émanant des établissements d'enseignement et de recherche français ou étrangers, des laboratoires publics ou privés.



# Preliminary results of Pyramid Piston Sensor calibration

Petr Janout<sup>a</sup>, Deborah Malone<sup>b</sup>, Ronald Holzlöhner<sup>a</sup>, Samuel Lévêque<sup>a</sup>, and  
Tomáš Fordey<sup>a</sup>

<sup>a</sup>European Southern Observatory, Garching, Germany

<sup>b</sup>Applied Optics, School of Physics, University of Galway, Ireland

## 1. ABSTRACT

Measurement of a phase difference between the mirror segments is a crucial task that we face nowadays when it comes to telescopes with segmented mirrors. From different perspectives, we need to be able to obtain the phase difference in a precise way. We don't need the phase measurement only for the adaptive optics, but the measurement can be used for the initial co-alignment of the mirror after the maintenance, for example. At ESO, we built a Pyramid Piston Sensor Test Bench for testing methods of discontinuous phase measurements. Original research based on experience with the GHOST bench was applied to the Pyramid Piston Sensor. The bench is equipped with a pyramid wavefront sensor with four facet pyramid and two different telescope simulators. The first telescope simulator emulates a segmented mirror using a Spatial Light Modulator. This telescope simulator is used for the calibration of the system. The other telescope simulator can host physical phase plates with known phase steps and is used for an actual measurement with the calibrated pyramid wavefront sensor. In this paper, we present the test bench and results of the calibration campaign, along with the description of findings noted during the calibration of the pyramid wavefront sensor.

## 2. INTRODUCTION

The Pyramid Piston Sensor (PPS) Test Bench evaluates and verifies the technique of measuring discontinuous phases. The Pyramid Wavefront Sensor similar to one used in the CaNaPy Laser Guide Star Adaptive Optics (LGS-AO) is used. The CaNaPy, which is a facility for studying novel visible (VIS) adaptive optics corrections, was first presented by Bonaccini in [1, 2]. The PPS aims to validate methods and algorithms for measuring discontinuous phases, such as those produced by misaligned segmented mirrors.

For small residual errors ( $< \pi/2$ ) single wavelength pyramid wavefront sensors can be used, while large errors would require other methods such as multiwavelength measurements [3]. Pyramid wavefront sensors (PWFs) could be used as an adjunct to segmented edge sensors [4], providing an additional method of differential piston detection, and can be used, for example, for initial alignment after replacement of a mirror segment.

For a segmented mirror, it is not possible to directly measure the phase difference between two segments using the pyramid wavefront sensor. However, there is a tent-like response signal in the slope centred over the

---

Further author information: (Send correspondence to P.J.)

P.J.: Email: petr.janout@eso.org

gap between the segments due to the discontinuity of the wavefront between them [3]. When using a modulated pyramid, the plot of tent peak height vs piston differential is sinusoidal, resulting in an ambiguous measurement once the optical path difference (OPD) exceeds +/- half a wavelength. For each sine period there are two possible values for the phase difference. To remove ambiguity, it is possible to use multiple wavelengths to calculate the most likely value. The work of Holzlöhner et al.[3] has shown that this method gives a good estimate of the true value of the phase difference. For small phase differences ( $\Delta\phi < \pi/2$ ) the use of a single wavelength is still a viable technique.

In the following sections, we recall our previous work on discontinuous phase detection and the recent results obtained on our test bench. First, we summarise the points covered in our previous work. Section 4 is devoted to an overview of the PPS test bench, the calibration of the PPS, and the algorithm used for phase retrieval. Section 5 describes the measured phase plates and shows the calibration curves obtained from the measurement with an SLM. The last section is devoted to the results.

### 3. PREVIOUS WORK

This work is based on previous experiments performed on the GPU-based High-order adaptive OpticS Testbench (GHOST) [5] at the European Southern Observatory (ESO) [6, 7]. GHOST is designed such that the sampling of the four pupils matches with the deformable mirror (DM). As such, the pupils are  $\approx 33$  pixels wide, to match with the DM's 24x24 actuator grid [8]. The SLM on the bench was used to generate phase screens with phase discontinuities of different amplitudes. The small number of pixels across the subaperture meant that only a few phase discontinuities could be accurately detected. Instead of one simulated segmented mirror with many phase discontinuities, many small sections were instead simulated. The slopes for each measurement were calculated according to Equations 1 & 2.

$$S_x = \frac{(I_1 + I_4) - (I_2 + I_3)}{(I_1 + I_2 + I_3 + I_4)} \quad (1)$$

$$S_y = \frac{(I_1 + I_2) - (I_3 + I_4)}{(I_1 + I_2 + I_3 + I_4)} \quad (2)$$

From the slopes, we generated data points of the signal across the edge vs the grey levels for each phase screen. Combined, these data points gave a calibration curve described by

$$f(\theta) = \frac{0.597 \sin \theta}{1 - 0.203 \cos \theta} \quad (3)$$

where  $\theta$  is the phase. As the SLM was calibrated to produce  $2\pi$  of phase change for a 770 nm laser over the 0-255 grey level range of the SLM, we converted the phase from grey levels to nanometres by multiplying the grey level values by  $\frac{770}{255}$  and using  $\theta = \frac{2\pi x}{770}$ .

The calibration curve was tested with three physical phase plates which have been manufactured with discontinuities of 131, 74, and 33 nm. These measurements were performed twice. In the initial measurement (dataset 1 in Figure 1), the introduction of the phase plates into the optical set-up introduced an unwanted tilt into the system due to the wedge shape of the plates. To compensate, the source LED was tilted. This introduced additional off-axis aberrations to the system, which made the measurements difficult. For the second dataset, a tilting mount was added, which could rotate the inserted phase plates to account for the tilt instead of adjusting the source. In both cases, blurred pupil images were used for brightness compensation. The results are shown in Figure 1.

Dataset 2 provided better results, in particular estimating a step of 132 nm for a real phase of 131 nm (Figure 1). However, it was determined that the GHOST bench was unsuitable for our specific use; the detection of very small phase steps. There simply was not enough resolution to accurately determine the location of the discontinuities, especially in the case of the 33 nm step, and residual aberrations made it difficult to measure. Therefore, this experiment is continued on the Pyramid Piston Sensor test bench, also being developed at ESO, which will provide a much higher spatial resolution than the GHOST bench, and is being developed solely for the determination of discontinuous phase steps with a pyramid wavefront sensor.

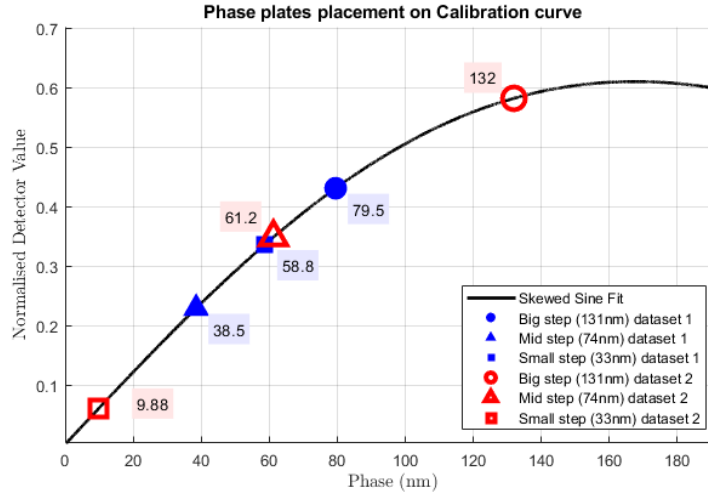


Figure 1: Interpolated positions of measured phase steps along the calibration curve. Unwanted aberrations in dataset 1 resulted in poor results. Addition of a rotating mount for dataset 2 improved the measurements for the 131 and 74 nm phase plates. 33 nm plate proved difficult to measure in both datasets.

## 4. CURRENT WORK

### 4.1 Design of the Pyramid Piston Sensor Test Bench

The Pyramid Piston Sensor Test Bench is based on the CaNaPy prototype of the Pyramid Wavefront Sensor (Py-WFS) module [2, 9]. The CaNaPy is a Laser Guide Star Adaptive Optics facility in development at ESO, in collaboration with The Australian National University (ANU), Istituto Nazionale di Astrofisica (INAF), Instituto de Astrofísica de Canarias (IAC), and Durham University. An overview of the PPS can be found in Figure 2. The core design concept is similar to that of CaNaPy Py-WFS, although PPS eliminates the need for high-speed and highly sensitive cameras. The PPS consists of readily available optics (mirrors and lenses), together with a specially designed glass pyramid, which splits the beam into two paths: the primary beam path to the glass pyramid, and the secondary path to the scoring camera. The pyramid sensor is identified as the main beam path camera, while the scoring camera captures 10% of the incoming light through a beam splitter (BS) on the light path.

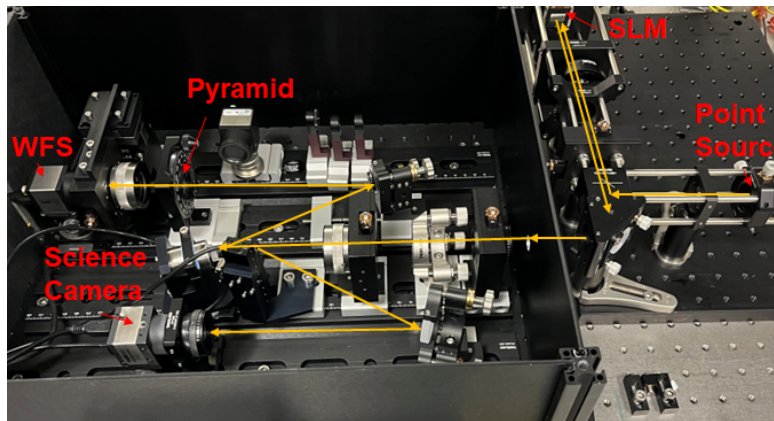


Figure 2: Pyramid Piston Sensor Test bench as set up at ESO. The bench equipment on the right containing the point source and the SLM is the telescope simulator, which can be modified to hold physical phase plates, either with or without the use of the SLM.

The incoming beam of light passes through the aperture and then passes through the first re-imaging lens. The BS, which is behind the first lens, reflects 10% of the light towards the folding mirror and the scoring camera, while the rest of the light is reflected by the tip/tilt mirror. The tip/tilt mirror is a  $\frac{1}{2}$ " mirror glued to the PI stage. After the tip/tilt stage, the beam is reflected by a folding mirror towards the pyramid. The pyramid is mounted on a rotary stage. An imaging lens then produces four pupil images on the OCAM camera sensor.

The PPS is illuminated by a telescope simulator using an SLM. The point source for the PPS is generated by a 589 nm light source, which then (optionally) travels to the SLM and then into the PPS itself. The PPS is modulated by a Physik Instrumente S-331 actuator driver, which consists of three actuators capable of modulating the beam at up to 2kHz. The pyramid has four facets and a roof angle of 7.2 degrees, and the beam passing through the pyramid is re-imaged onto the WFS camera through a 50 mm lens. The pupils on the detector camera are  $\approx 160$  pixels in diameter.

The signals to the actuators had to be set to slightly different voltages to achieve circular modulation. The relationship between the two signal voltages and modulation radius can be seen in Figure 3, where the necessary voltages are marked for a modulation radius of  $3\lambda/D$ , which will be used in experiments. The modulation frequency is chosen as 500Hz.

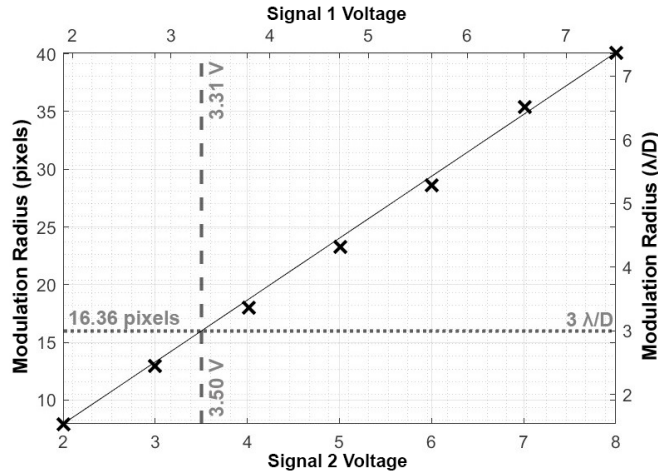


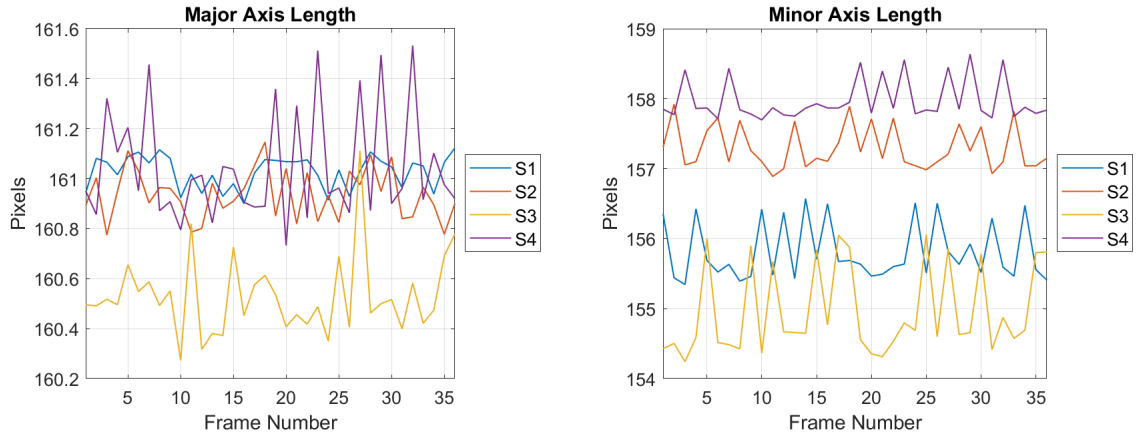
Figure 3: Relationship between signal voltages and modulation radius. the x's show the resulting modulation radius in pixels for given signal voltages. The diagonal line shows this as a linear relationship, given by  $y = 5.3651x - 2.7967$ . The graph can be used to determine the required voltages for a given  $\lambda/D$ . Shown here in the dotted lines for a circular modulation radius of  $3\lambda/D$ , we see signal 1 must be set to 3.31 V, while signal 2 must be 3.5 V, shown by the dashed line.

The major and minor axes of each subaperture were also measured over several frames. These measurements are shown in Figure 4.

## 4.2 Software

To control the bench, a Graphical User Interface (GUI) was developed in MATLAB, which allows the user to align the pupil images and view the resulting x- and y-slopes in real time. Once the pupils are aligned, the user can then mark the edges on the images. For calibration data, the signal from the slopes is recorded along with the grey level difference which produced it, which is then converted to a nanometre value and used to produce a calibration curve. For measurement data, the previously generated calibration curve is used to estimate the phase difference. An example of the software is shown in Figure 5.

This iteration of the calibration curve calculating algorithm handles the signals from the edge differently. Previously, the value was taken as a single point in the centre of the edge. Now, the value is taken as the average along the edge.



(a) The length of the major axis of each subaperture between subsequent images. (b) The length of the minor axis of each subaperture between subsequent images.

Figure 4: The length of the major and minor axes of each subaperture over a 36 image sequence is shown here. Average major axis length is  $160.88 \pm 0.26$  pixels. Average minor axis length is  $156.51 \pm 1.27$  pixels. Average eccentricity for the pupils is 0.23.

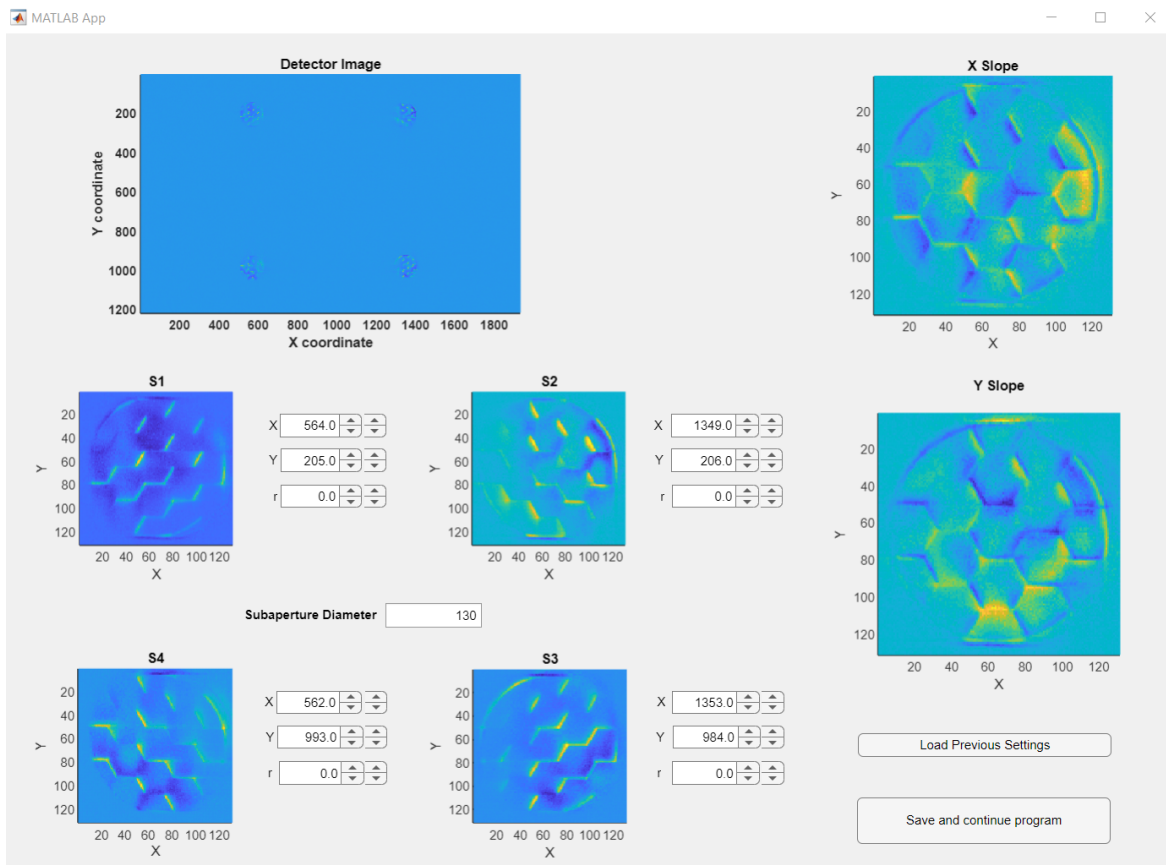


Figure 5: The Graphical User Interface (GUI) for analysing the images taken by the detector on the PPS. This allows the user to find and align the four subapertures while being able to see the resulting slopes images in real time.

## 5. MEASUREMENTS

### 5.1 Calibration Curve

The calibration curve is obtained from a series of measurements using the SLM. We generated phase screens with multiple phase discontinuities with the same grey level difference in the range of 0 to 589 nm. The brightness was once again compensated via the subtraction of blurred pupil images. The calibration curve was then obtained from the slopes paired with the known value of the phase screen. The standard deviation of these signals is used as the measurement error. The curve is shown in Figure 6.

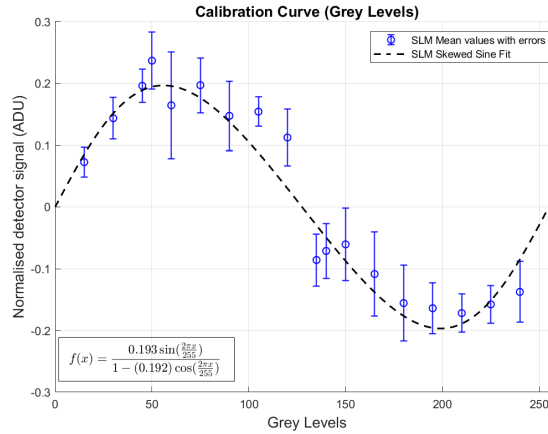


Figure 6: The calibration curve produced by using phase screens with one screen containing multiple phase discontinuities, with either hexagonal or chequerboard phase screens. The error bars show the scatter of the calibration points measured on a single phase screen.

### 5.2 Physical Phase Plates

The calibration curve from Figure 6 is converted to nanometres assuming that 255 grey levels is equal to 589 nm, and is used to estimate the phase discontinuities from the three physical phase plates used in the previous work [7], summarised in Section 3. Initially, this measurement was performed without the SLM in place. The PyWFS images of the phase plates were extremely sharp, with the edge clearly defined and easy to measure. However, the signal from these images was much higher than the signal from the edges produced by the SLM, and this can be seen in Figure 7.

As the signal was much higher, it was decided to re-take the measurements with the SLM in place. Due to the wedge shape of the phase plates, and the additional reflection from the SLM, two edges are visible in the detector image. This can be seen in Figure 8. With the SLM in place, the signal matches reasonably well with the calibration curve. The data points for the known phase difference are shown in Figure 9a. Note that the signal for each edge when vertical and horizontal are given in this figure.

## 6. RESULTS

### 6.1 Phase Estimation

Assuming that the phase discontinuity of the phase plates is unknown, what would the calibration curve estimate the values to be? For this, the values from the phase plates in a horizontal and vertical position are averaged, and the standard deviation of the two measurements is used as an error. These signal values are then compared to the calibration curve to estimate the phase step values in nanometres.

In Figure 10, the extrapolated values are shown on the graph and in Table 1. The curve estimates a value of 34.92 for 33 nm, 70.95 for 74 nm, and 129.36 for 131 nm. The signal for the 131 nm phase screen is higher than the amplitude of the calibration curve; therefore, the closest possible value is the tip of the curve itself.

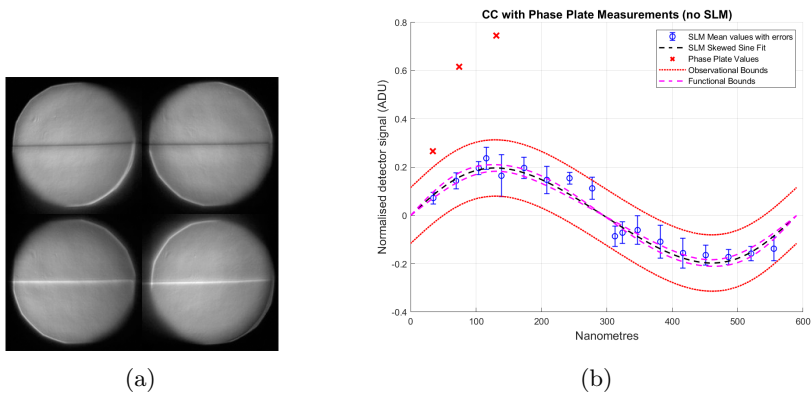


Figure 7: Detector image of the 131 nm phase plate (left) taken without the SLM in place, with the resulting data points overlaid on the calibration curve (right). Included in the calibration curve are the observational and functional bounds, which correspond to the confidence levels that new observations belong to the data set (observational bounds), and that the true calibration curve lies within the area given by the functional bounds, which takes into consideration the uncertainty in the amplitude and skew of the sine fit.

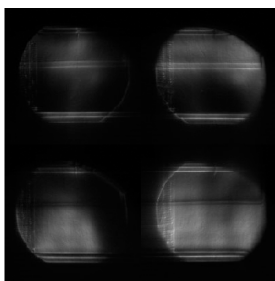


Figure 8: Detector image of the 131 nm phase plate taken with the SLM in place.

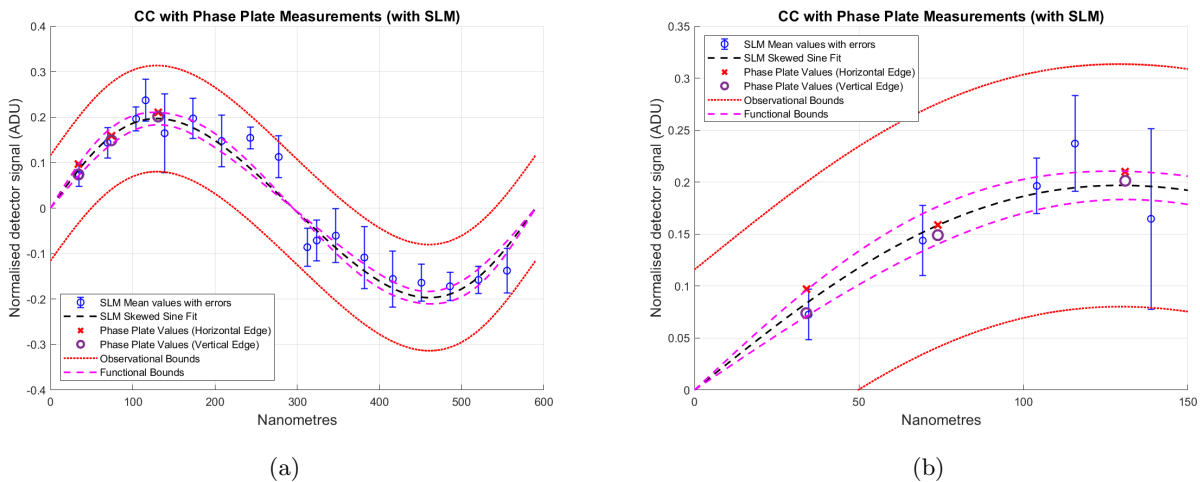


Figure 9: The resulting data points overlaid on the calibration curve (left), with a zoom in on the phase plate data (right)

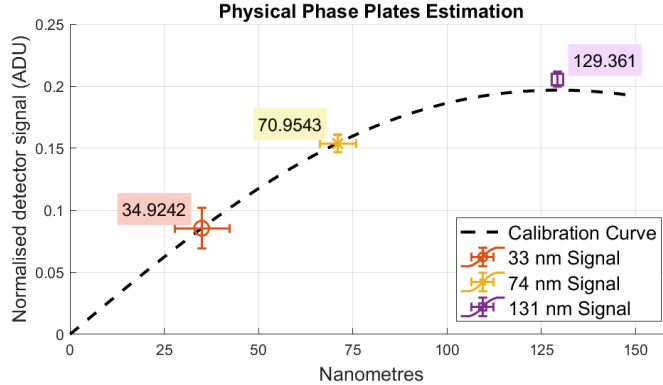


Figure 10: Extrapolated phase results from the phase plate measurements. From left to right, 33, 74, and 131 nm estimates. The vertical error bars correspond to the standard deviation in the measurements, while the horizontal error bars represent the phase uncertainty resulting from the signal measurement deviation.

Table 1: Estimated values of phase for the signals from each of the three phase plates. The upper and lower limits refer to the maximum and minimum phase values the signal could correspond too according to the error in that signal.

Step (nm)	33	74	131
Mean Signal	$0.085 \pm 0.016$	$0.154 \pm 0.007$	$0.206 \pm 0.006$
Constrained Curve Results			
Est. Phase (nm)	34.92	70.95	129.36
Upper Limit (nm)	42.33	75.90	129.36
Lower Limit (nm)	27.88	66.38	129.36

## 7. CONCLUSION

In this paper, we present the current findings on measuring known physical phase plates using the Pyramid Piston Sensor Test Bench. Our objective was to verify the PPS calibration using an SLM screen and enable the calibration tool to measure the discontinuous phase steps. A calibration curve was produced relating the phase difference to the sensor signal. This curve can be employed as a reference to determine the phase difference of a known or unknown discontinuity for a given detector value. Note that SLM calibration using the PPS remains unconvincing due to the high wavefront error of the SLM display. Even in a single measurement, where only one phase step was introduced, the calibration points exhibit a significant dispersion (error bars in Figure 6). The calibration curve is fitted to the mean point of each measurement. The SLM’s residual phase error, which could not be calibrated out, forced us to use the SLM for both the calibration curve and the actual measurement of the physical phase plates. Although constructing the SLM calibration curve was challenging, we were able to obtain accurate measurements of the phase plates without atmospheric turbulence. Additionally, comparing the presented phase plate measurement with that performed on the GHOST bench demonstrated an enhanced characterisation of the phase plates. In conclusion, it is preferable to employ a set of known physical phase plates to define the calibration curve in future work, as the SLM did not show the required accuracy of the PPS calibration. The implementation of physical phase plates also revealed adequate contrast for PPS measurement.

## 8. ACKNOWLEDGEMENTS

This work has been supported by the Irish Research Council under the Government of Ireland Postgraduate Scholarship Programme (Project ID GOIPG/2020/537) and the European Southern Observatory Studentship Programme.

## References

- [1] D. Bonaccini Calia et al. “CaNaPy: SatComm LGS-AO experimental platform with laser uplink pre-compensation”. In: *International Conference on Space Optics — ICSO 2020*. Ed. by Bruno Cugny, Zoran Sodnik, and Nikos Karafolas. Vol. 11852. International Society for Optics and Photonics. SPIE, 2021, pp. 536–546. DOI: [10.1117/12.2599233](https://doi.org/10.1117/12.2599233). URL: <https://doi.org/10.1117/12.2599233>.
- [2] Domenico Bonaccini Calia et al. “CaNaPy: LGS-AO experimental facility for visible wavelengths”. In: *Adaptive Optics Systems VIII*. Ed. by Laura Schreiber, Dirk Schmidt, and Elise Vernet. Vol. 12185. International Society for Optics and Photonics. SPIE, 2022, p. 121857L. DOI: [10.1117/12.2630337](https://doi.org/10.1117/12.2630337). URL: <https://doi.org/10.1117/12.2630337>.
- [3] Ronald Holzlöhner et al. “Maximum likelihood co-phasing of segmented mirrors with a pyramid in the visible: simulation vs. experiment”. In: *Adaptive Optics Systems VII*. Vol. 11448. SPIE. 2020, 114480S. URL: <https://doi.org/10.1117/12.2563287>.
- [4] Simone Esposito et al. “Pyramid sensor for segmented mirror alignment”. In: *Optics letters* 30.19 (2005), pp. 2572–2574. URL: <https://doi.org/10.1364/OL.30.002572>.
- [5] Markus Kasper et al. “PCS–A Roadmap for Exoearth Imaging with the ELT”. In: *arXiv preprint arXiv:2103.11196* (2021). URL: <https://doi.org/10.48550/arXiv.2103.11196>.
- [6] Deborah Malone et al. “Detection of discontinuous phase steps with a pyramid wavefront sensor”. In: *Adaptive Optics Systems VIII*. Vol. 12185. SPIE. 2022, pp. 1643–1655. URL: <https://doi.org/10.1117/12.2632347>.
- [7] Deborah Malone et al. “Pyramid Wavefront Sensors for the Detection of Small Phase discontinuities”. In: *Wavefront Sensing in the VLT/ELT era VII*. 2022. URL: <https://wfs2022.sciencesconf.org/426139>.
- [8] Byron Engler et al. “The GPU-based High-order adaptive OpticS Testbench”. In: *Adaptive Optics Systems VIII*. Vol. 12185. SPIE. 2022, p. 1218558. URL: <https://doi.org/10.1117/12.2630595>.
- [9] Petr Janout et al. “CaNaPy facility: opto-mechanical design and requirements for optimal visible systems LGS-AO”. In: *Ground-based and Airborne Telescopes IX*. Ed. by Heather K. Marshall, Jason Spyromilio, and Tomonori Usuda. Vol. 12182. International Society for Optics and Photonics. SPIE, 2022, p. 1218226. DOI: [10.1117/12.2629266](https://doi.org/10.1117/12.2629266). URL: <https://doi.org/10.1117/12.2629266>.